Structure and magnetism in Dy_xPr_{1-x} and Er_xPr_{1-x} alloys: II. Double-hexagonal close-packed structure

2001 J. Phys.: Condens. Matter 13 10191

(http://iopscience.iop.org/0953-8984/13/45/307)

INSTITUTE OF PHYSICS PUBLISHING JOURNAL OF PHYSICS: CONDENSED MATTER

J. Phys.: Condens. Matter **13** (2001) 10191–10206 PII: S0953-8984(01)24948-0

Structure and magnetism in Dy_xPr_{1-x} and Er_xPr_{1-x} alloys: II. Double-hexagonal close-packed structure

P S Clegg[1,5], R A Cowley[1], J P Goff[2], D F McMorrow[3], M Sawicki[4,6], R C C Ward[1] and M R Wells[1]

[1] Oxford Physics, Clarendon Laboratory, Oxford OX1 3PU, UK
[2] Department of Physics, University of Liverpool, Oliver Lodge Laboratory, Liverpool L69 7ZE, UK
[3] Department of Solid State Physics, Risø National Laboratory, Roskilde DK-4000, Denmark
[4] Department of Physics and Astronomy, University of Southampton, Southampton SO17 1BJ, UK

E-mail: clegg@physics.utoronto.ca

Received 17 May 2001
Published 26 October 2001
Online at stacks.iop.org/JPhysCM/13/10191

Abstract

The structure and magnetism of epitaxial thin-film dysprosium–praseodymium and erbium–praseodymium alloys with the double-hexagonal close-packed (dhcp) crystal structure have been investigated. Short-range atomic and magnetic order have been found for Dy_xPr_{1-x} with $0.4 \geqslant x \geqslant 0.05$ and Er_xPr_{1-x} with $0.2 \geqslant x \geqslant 0.05$. The distribution of the two species within the alloys was established with x-ray and neutron diffraction techniques. The atomic order is complex; the four planes of the unit cell have differing concentrations of constituents. In addition there are occasional clusters within the close-packed planes. The magnetic behaviour was investigated using neutron diffraction. Surprisingly, only short-range order is observed in the dhcp-structure alloys. Magnetization measurements suggest that $Dy_{0.13}Pr_{0.87}$ exhibits spin-glass behaviour. The roles of the indirect exchange interaction, the dipole–dipole interaction and the crystal field are considered in detail.

1. Introduction

In this paper we report neutron diffraction, x-ray diffraction and magnetization studies of epitaxial thin films of dhcp-structure Dy_xPr_{1-x} and Er_xPr_{1-x} alloys. The dhcp crystal structure exists over the range $0.4 \geqslant x \geqslant 0$. The results indicate that the magnetism is due to competition between different two-ion interactions. It has been found that the anisotropy created by the

[5] Present address: Department of Physics, University of Toronto, Toronto, Ont. M5S 1A7, Canada.
[6] Present address: Institute of Physics, Alica Lotnikow 32/46, 02-668 Warszawa, Poland.

crystal field has a significant effect on the range of the magnetic order established by the system. The alloys also exhibit short-range atomic order.

The magnetic ordering temperatures are lowest at the beginning of the rare-earth period: the light rare earths are exposed to greater influence from the crystalline field due to the f-shell electrons being less tightly bound to the nucleus compared to the heavy rare earths. Additionally the exchange interaction tends to be weaker. The size of the spin–spin interaction is related to the de Gennes factor $y = (g-1)^2 J(J+1)$. In the light rare earths g is just a little less than one, making y small. This is a consequence of the $\boldsymbol{J} = |\boldsymbol{L} - \boldsymbol{S}|$ configuration at the beginning of the period. The behaviour described here is unlike that of the hcp- and Sm-structure alloys described in the previous paper [1]. The hcp alloys exhibit magnetism similar to that of the heavy rare earths: the indirect exchange is relatively strong, being only weakly perturbed by the crystal field. Magnetoelastic effects were also important for the hcp alloys whereas they are far less so for the dhcp alloys.

The alloys studied in this work are praseodymium based. Pr is a singlet-ground-state system which is very close to the threshold at which the exchange interaction induces a moment [2]. Three factors lead to the singlet ground state in Pr:

(1) The crystal-field effect is large compared to the exchange interaction.
(2) The strong spin–orbit coupling in the rare earths implies that, although the crystal field acts on the orbital component of the moment, the total moment responds.
(3) Pr is a non-Kramers ion.

Perturbations such as the hyperfine coupling, applied pressure and the addition of magnetic impurities can tip the balance such that a permanent moment is induced at very low temperatures. The hyperfine coupling induces long-range magnetic order at $T \sim 45$ mK [3]. The moments on the hexagonal sublattice of the dhcp structure order to form an incommensurate modulation along $\boldsymbol{a}^*$ with the hexagonal planes antiferromagnetically aligned.

As solutes, the ions of the heavy rare earths Dy and Er are slightly smaller than those of their host, and have large saturated magnetic moments (10 μ_B and 9 μ_B respectively). Both are Kramers ions. Dy tends to exhibit basal-plane anisotropy in a hexagonal crystal field; Er has uniaxial anisotropy under the same circumstances [4]. As the elements are from the second half of the period, Hund's rule gives rise to a total moment of the form $\boldsymbol{J} = \boldsymbol{L} + \boldsymbol{S}$.

In light–heavy-rare-earth alloys there is a difference between the moments coupled by the indirect exchange and the magnetic moments coupled by other interactions such as the classical dipole–dipole interaction. The indirect exchange is the interaction between the localized spins via the polarization of the conduction electrons. It can be expressed in terms of the total spins of the two interacting ions. Since the total angular momentum $\boldsymbol{J}$ is a constant of the motion for rare earths, the total spin is most usefully written as $\boldsymbol{S} = (g-1)\boldsymbol{J}$ where g is the Landé factor. It should be noted that the relative orientation of $\boldsymbol{S}$ and $\boldsymbol{J}$ changes from antiparallel to parallel halfway across the period as g goes from being less than one to greater than one. By contrast the dipole–dipole interaction couples the total moment $g\boldsymbol{J}$. The size of the moment changes across the period, however there is no sudden change of orientation. To summarize:

$$\text{indirect exchange depends on} \quad (g-1)\boldsymbol{J} \qquad \begin{cases} (g-1) < 0 & \text{light} \\ (g-1) > 0 & \text{heavy} \end{cases} \tag{1}$$

$$\text{dipole–dipole interaction depends on} \quad g\boldsymbol{J} \qquad g > 0 \text{ when } J > 0. \tag{2}$$

This difference becomes significant for alloys of light rare earths with heavy rare earths. When moments from opposite halves of the period interact, the indirect exchange will oppose the

dipole–dipole interaction. For systems in which the indirect exchange is weak, this can lead to frustration.

Pre-1984 experimental work on light–heavy-rare-earth alloys is reviewed in reference [5]. Subsequent studies of particular interest include those concerning excitations [6, 7] and those involving epitaxial systems [8–10]. The current research was undertaken to investigate the complete suppression of magnetism in the $x = 0.2, 0.3$ Ho_xPr_{1-x} dhcp alloys [9]. Since the ($x = 0.0$) Pr film orders magnetically with a slightly elevated transition temperature, it is apparent that the magnetism is not suppressed as a result of epitaxy. It was hoped that, by replacing Ho with Dy or Er, it would be possible to gain an improved understanding of the behaviour of the dhcp light–heavy-rare-earth alloys. Both Dy and Er are Kramers ions which removes the possibility of the system adopting a singlet ground state. Additionally, the anisotropies of Dy and Er in a hexagonal crystal field are different, being easy planar and uniaxial respectively. Studying the behaviour of both systems may assist in characterizing the interactions which are important in the dhcp alloys.

In interpreting the results it is necessary to understand spin-glass behaviour and superparamagnetism:

(i) A spin glass is a magnetic system with an unusual phase transition at a temperature T_g. Below T_g the magnetic moments are frozen in random orientations without conventional long-range order. For a system to be a spin glass, the necessary conditions are randomness and competing interactions [11]. No moment configuration can minimize all the interaction energies (frustration) and the result is very many stable configurations. Since the energies are very similar, the configuration that the spin glass freezes into depends on the history of the system. The symmetry which is being broken at the spin-glass freezing transition is ergodicity: the ergodic hypothesis holds that in equilibrium any system should be found with probability $e^{-\beta E}$ in any of its possible configurations. A spin glass exhibits non-trivial broken ergodicity [12] corresponding to the system having very many stable states. Spin glasses are normally identified using dc and ac susceptibility, specific heat or resistivity measurements [11]; however, it is often possible to observe short-range order using neutron scattering techniques [13].

(ii) A superparamagnet is an assembly of single-domain particles in thermal equilibrium. The properties are similar to those of an atomic paramagnet except that the single-domain particle contains $\sim 10^5$ atoms coupled by exchange interactions. The single-domain *particles* are considered non-interacting; hence magnetization measurements should show Curie-law behaviour.

This paper is organized as follows. Sample growth issues are outlined in section 2. Structural and magnetic experimental results for the two systems are contained in section 3 and show that the magnetic behaviour of some of the samples is dominated by short-range magnetic order. The role of the dipole–dipole interaction is considered in section 4. The structural, magnetic and model results are discussed in section 5.

2. Sample growth

The samples were grown by molecular-beam epitaxy using a Balzers UMS 630 facility in the Clarendon Laboratory, Oxford. The growth techniques are similar to those developed for Ho_xY_{1-x} alloys [15]. Experiments were carried out on Dy_xPr_{1-x} with $x = 0.05$, 0.13, 0.2, 0.3, 0.4 and Er_xPr_{1-x} with $x = 0.05, 0.1, 0.2$. Larger (20×22 mm^2) sapphire substrates were employed for the dhcp alloys than for the hcp- and Sm-structure alloys described in the previous paper [1]. The reason for this larger size is that the magnetic moment in the dhcp

systems tends to be smaller; more material is required to obtain a significant magnetic neutron scattering signal. The buffer layer and seed layer combinations are described below. For the alloys, the deposition rate was 1 Å s^{-1}, controlled to provide the designated composition. The alloys were grown to a thickness of 10 000 Å. For all samples a cap of Nb or Y was added for general protection and to reduce reaction with the atmosphere.

Three combinations of buffer and seed layer were used. The first series of samples were grown with 1000 Å of Nb as the buffer layer with no additional seed layer. The second series had 100 Å of Nb and 1250 Å of Y as a seed layer. The amount of Nb was reduced since some of these samples were intended for use in magnetization measurements. The third series had 1000 Å of Nb and 1000 Å of Y. The characteristics of the dhcp samples demonstrate the importance of the buffer layer in the growth of high-crystalline-quality films. For dhcp samples with a thick (∼1000 Å) layer of Nb, the mosaic spread was $\Delta\theta \sim 0.18^\circ$ and the plane-spacing coherence length was $\xi \sim 1200$ Å. Samples with a 100 Å buffer layer had $\Delta\theta \sim 0.31^\circ$ and $\xi \sim 245$ Å. Evidently it is the thickness of the buffer layer, far more than that of the seed layer, which is determining the crystal quality. Work on the epitaxial growth of semiconductors [16] shows that a film thicker than t_c, with a lattice mismatch to the crystal surface on which it is being grown, forms dislocations to relieve the strain. The value of t_c depends on the lattice mismatch. Above t_c the film will relax towards its bulk lattice parameters. It appears likely that for Nb grown on sapphire, t_c falls between 100 Å and 1000 Å, and that the strain in the buffer layer is influencing the crystalline quality of the rare-earth film.

3. Experimental results

The samples were examined at the Clarendon Laboratory, Oxford, using high-resolution x-ray diffractometers. Neutron scattering experiments were undertaken at the Risø National Laboratory, using the triple-axis spectrometer TAS1. The alloys were clamped in a variable-helium-flow cryostat for measurements between $T = 100$ K and $T = 1.8$ K. The temperature was measured to an accuracy of ± 0.1 K. Pyrolytic graphite crystals were used as a monochromator and an analyser, both being aligned to reflect 5 meV neutrons, and a cooled beryllium filter was employed to reduce higher-order contamination of the incident neutron beam. The bulk magnetization properties of one of the samples was studied using the vibrating-sample magnetometer at Southampton University. The temperature range for these measurements was 2 K to 25 K.

3.1. Structural properties

The x-ray scattering for a wave-vector transfer along $[1\,0\,q_l]$ indicates that the stacking sequence for all samples is dhcp, uncontaminated by other phases. The plane-ordering coherence length as determined from the FWHM of the Bragg peaks along $[1\ 0\ q_l]$ was $\xi \sim 250$ Å. For consistency with the previous paper [1], the reflections are indexed throughout using the hcp reciprocal cell.

Figure 1 shows the scattering for $\boldsymbol{Q}$ along $[0\,0\,q_l]$ for $Dy_{0.05}Pr_{0.95}$, a sample with the dhcp crystal structure. Only the (0 0 2) peak is anticipated along $[0\,0\,q_l]$; however, the dhcp alloys have additional superlattice peaks at (0 0 1/2), (0 0 1) and (0 0 3/2) as well. The dhcp unit cell consists of four planes ordered as ABAC, where the A planes have approximately cubic local symmetry whereas the B and C planes have approximately hexagonal local symmetry. The extra peaks indicate that either the two constituents are not randomly distributed on each plane but have preferred sites within the unit cell or that the lattice parameters are systematically deformed. To test which of these two hypotheses is most likely to be correct, the variation

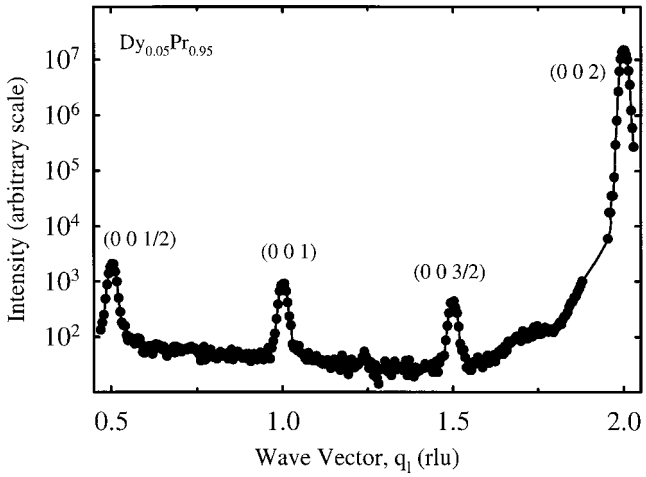

Figure 1. X-ray scattering intensity measured in a scan of $\boldsymbol{Q}$ along the [0 0 q_l] direction for $Dy_{0.05}Pr_{0.95}$ at room temperature. Only the (0 0 2) peak is anticipated for a uniform dhcp alloy. For consistency with the previous paper [1], the reflections are indexed throughout using the hcp reciprocal cell.

of intensity with concentration changes and distortions has been modelled. The plane form factor f_n and position x_n are

$$f_n = \overline{f} + f' \cos(nk\overline{x}) + f'' \cos\left(\frac{1}{2}nk\overline{x}\right) \tag{3}$$

$$x_n = n\overline{x} - x' \sin(nk\overline{x}) - x'' \sin\left(\frac{1}{2}nk\overline{x}\right) \tag{4}$$

where n is the plane index, $k = \pi/d$ is the modulation wave vector and d is the plane separation. The average values of the form factor and the position are $\overline{f}$ and $\overline{x}$ respectively. The amplitudes of the two-plane and four-plane modulations are f', x' and f'', x''. Taking an ion for which f_n is maximum, the choice of expression for x_n means that the neighbouring planes x_{n-1} and x_{n+1} will be closer than the average ($\overline{x}$) to plane n. Such an assignment is appropriate since the heavy-rare-earth ions are smaller but scatter more strongly than the light-rare-earth ions. The scattering intensity can be found from the Fourier transform of this modulation. The only approximation is to expand the exponential of the small position modulation as a series for which second-order and higher terms can be neglected. This gives the intensity variation as

$$I(q) = \frac{2\pi N}{\Omega} \sum_{\tau} \overline{f}^2 \delta(q-\tau) + \frac{1}{4}(f' + q\overline{f}x')^2 \delta(q-k-\tau) + \frac{1}{4}(f' - q\overline{f}x')^2 \delta(q+k-\tau)$$
$$+ \frac{1}{4}(f'' + q\overline{f}x'')^2 \delta\left(q - \frac{k}{2} - \tau\right) + \frac{1}{4}(f'' - q\overline{f}x'')^2 \delta\left(q + \frac{k}{2} - \tau\right)$$

where q is the wave-vector transfer and τ is a reciprocal-lattice vector. The first delta function corresponds to the usual Bragg peak, while another four peaks arise due to the concentration and strain modulation. Changes in concentration alone give q-independent scattering while distortions alone give an intensity proportional to q^2. The model has been compared to the x-ray scattering for four samples, $Dy_{0.05}Pr_{0.95}$, $Dy_{0.13}Pr_{0.87}$, $Er_{0.05}Pr_{0.95}$ and $Er_{0.2}Pr_{0.8}$. Pairs of superlattice reflections with the same structure factor but with significantly different q-values

were chosen. These were the (0 0 1) with the (0 0 3) and the (0 0 3/2) with the (0 0 7/2). Due to the differences in wave-vector transfers it was especially important to correct for the q-dependence of the form factor, the Lorentz factor and the polarization factor. The latter corresponds to x-ray measurements made in the two-axis configuration with a Ge(1 1 1) monochromator. Figure 2 shows that the q-dependence is small and inconsistent for the corrected peaks. Comparing this result with the model suggests that x' and x'' are zero, the superlattice peaks being due to variations in concentration. Assuming that concentration modulation is the only cause, the two-plane effect gives $f' \sim 2\%$ while the four-plane effect is $f'' \sim 1\%$ of the average $\overline{f}$. f' represents the change in form factor between the cubic and hexagonal symmetry sites in the dhcp crystal structure. The result is consistent with the heavy-rare-earth ions preferentially occupying hexagonal symmetry sites. This is expected since the heavy rare-earth metals prefer the hcp crystal structure. The occurrence of a non-zero f''-term is more of a surprise. It indicates that either the two cubic planes have different populations of the two species or alternatively the imbalance occurs for the two hexagonal planes.

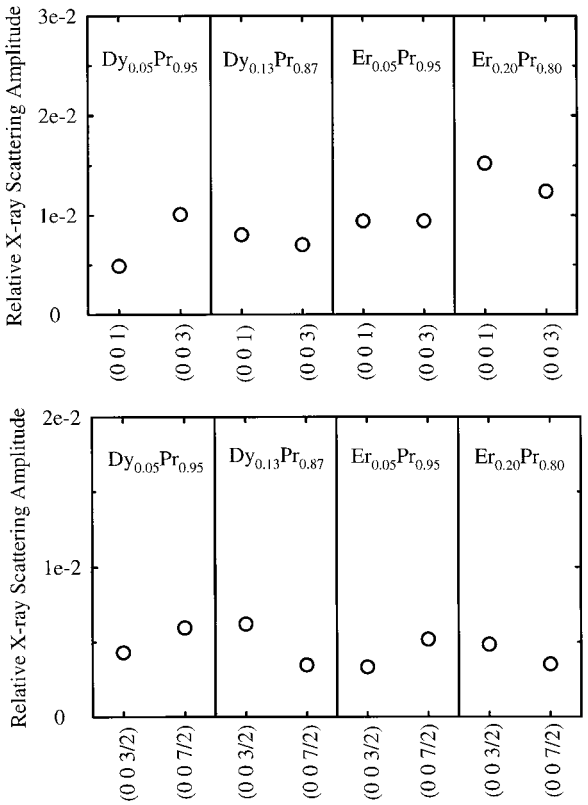

Figure 2. X-ray scattering amplitude for superlattice peaks relative to the (0 0 2) peak in the dhcp-structure alloys. The data have been corrected for the q-dependent form factor, the Lorentz factor and the polarization effect. The scattering amplitude appears to have no consistent q-dependence indicating that the peaks are likely to be due to concentration variations.

Neutron scattering measurements provide further structural information on the dhcp alloys, since the contrast between the scattering lengths of the two constituents is quite large and the resolution function is considerably broader, aiding the measurement of weak diffuse scattering. The dhcp alloys exhibit a temperature-independent ridge along the [0 0 q_l]; see for example

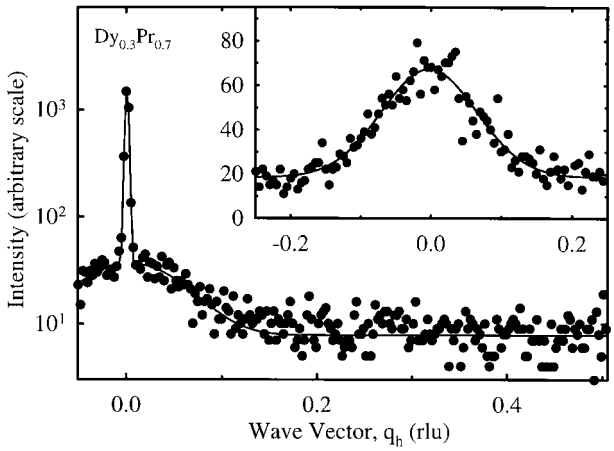

Figure 3. Neutron scattering intensity measured in a scan of $\boldsymbol{Q}$ along the $[q_h\ 0\ 1]$ direction for $Dy_{0.3}Pr_{0.7}$ at 30 K. This shows the sharp superlattice peak and the broad ridge. Inset is a scan across the ridge at $[q_h\ 0\ 3/2]$.

figure 3. This diffuse scattering pattern clearly indicates the presence of uncorrelated disorder that concerns crystallographic planes perpendicular to the c-axis. It is possible that the two species have a non-random distribution on the sites in the basal plane. Two arrangements are, firstly, that where an ion of a particular species tends to be surrounded by ions of the other species giving ordering and, secondly, that where an ion of a particular species tends to be surrounded by ions of the same species, giving clustering. If ordering were occurring, it would be anticipated that an array of columns of diffuse scattering would exist corresponding to the structure factor of the plane. This has not been observed in the $(q_h\ 0\ q_l)$ plane. Nor have additional sharp superlattice reflections been observed, despite extensive searches in reciprocal space using x-rays. It seems there is no tendency for the two species to order within the plane and that the diffuse column is due to clustering. Small domains, rich in one of the constituents, are randomly distributed within the domains. Uncorrelated changes in plane spacing occur associated with the domains due to the different sizes of the two ions. The plane-spacing changes occur in domains whose size can be estimated from the in-plane FWHM of the column to be $\sim$20 Å.

The x-ray results have shown that there is long-range order in the distribution of constituents on the sites of differing symmetry. The neutron scattering results have shown that there is a tendency for clusters, rich in a particular constituent, to be randomly distributed within some of the planes.

The chemical behaviour implied by the x-ray and neutron results has similarities to a pre-precipitation phase known to occur in the alloys Cu_xAl_{1-x}, Mn_xAl_{1-x} and others [17, 18]. These alloys are solid solutions which have a preferred composition or solubility limit. If a solid solution is fabricated which is supersaturated, then in equilibrium it would consist of a depleted matrix with a concentration of atoms equal to the solubility limit and a precipitate into which the excess atoms have collected. Various alloys including Cu_xAl_{1-x} and Mn_xAl_{1-x} have a metastable pre-precipitate phase. The excess dissolved atoms tend to form clusters or zones. The essential characteristic of a zone which justifies making a distinction between it and a very small precipitate is that it has perfect coherence with the lattice of the matrix. The zone is a crystalline irregularity in composition and, if the atoms have different sizes, in displacement. The zones (called Guinier–Preston zones [18]) lead to a column of diffuse

scattering, while an ordered matrix could be anticipated to give sharp superlattice features. Heat-of-mixing data for light–heavy-rare-earth alloys [19] indicate that there is likely to be an optimum concentration in the dhcp regime.

3.2. Magnetic properties

The magnetic behaviour determined using neutron scattering and a magnetization measurement are summarized in table 1. Where magnetic neutron scattering has been observed it has been centred around (q_h 0 3/2) positions in reciprocal space. The values of q_h have been tabulated along with the temperatures at which magnetic order began. The two systems will be discussed separately.

Table 1. Magnetic order in the dhcp alloys.

Sample	q_h (rlu)	T_N (K)	Technique
$Dy_{0.05}Pr_{0.95}$	—	—	Neutrons
$Dy_{0.13}Pr_{0.87}$	Not known	12 ± 1	Magnetization
$Dy_{0.2}Pr_{0.8}$	Not known	>1.8	Neutrons
$Dy_{0.3}Pr_{0.7}$	0.061 ± 0.002	>1.8	Neutrons
$Dy_{0.4}Pr_{0.6}$	0.066 ± 0.002	30 ± 2	Neutrons
$Er_{0.05}Pr_{0.95}$	0.202 ± 0.002	3.4 ± 0.5	Neutrons
$Er_{0.1}Pr_{0.9}$	0.205 ± 0.002	3.5 ± 0.5	Neutrons
$Er_{0.2}Pr_{0.8}$	—	—	Neutrons

3.2.1. Dy_xPr_{1-x}. The magnetic scattering observed for $\boldsymbol{Q} \sim (q_h\ 0\ 3/2)$ from $Dy_{0.4}Pr_{0.6}$ is shown in figure 4(a); a temperature-independent background, similar to that shown in figure 3, has been subtracted. The temperature dependence of the integrated intensity of the magnetic scattering is shown in figure 4(b). The ordering temperature deduced from these results is 30 ± 2 K. At 1.8 K the magnetic correlation lengths in the $\boldsymbol{c}^*$-direction and in the basal plane are 100 ± 10 Å and 64 ± 6 Å respectively. This indicates that the magnetic order is quite short range. The magnetic reflections are at a somewhat smaller modulation wave vector

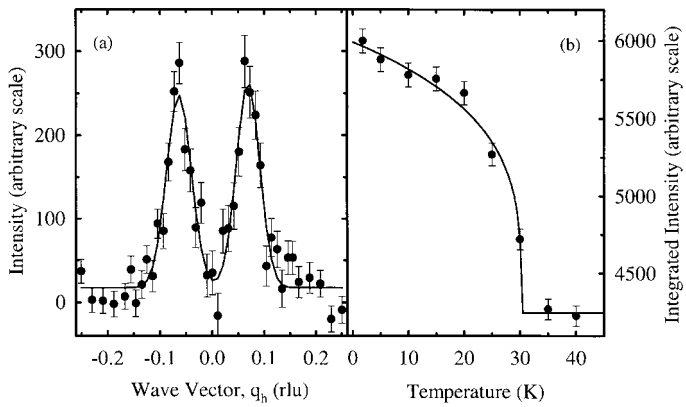

Figure 4. (a) The magnetic scattering observed for $\boldsymbol{Q} \sim (q_h\ 0\ 3/2)$ from $Dy_{0.4}Pr_{0.6}$. (b) The temperature dependence of the peak intensity, showing that the ordering temperature is 30 ± 2 K.

($q_h = 0.066 \pm 0.002$ rlu) than that of elemental Pr at millikelvin temperatures ($q_h = 0.128$ rlu). The ordering wave vector of the alloys increases very slightly with increasing temperature. Broad neutron scattering peaks with $q_l = 3/2$ rlu correspond to short-range order on two out of four of the planes in the unit cell. Furthermore, this location in reciprocal space indicates that the moments on successive ordered planes are antiferromagnetically aligned. It seems reasonable to assume by analogy with Pr and the highest-temperature ordered structures of Nd that it is the moments on hexagonal symmetry sites which exhibit the short-range order.

Figure 5 shows that the alloys with $x = 0.3$ and $x = 0.2$ (inset) may exhibit similar short-range magnetic order. The temperature-dependent scattering observed in these systems is consistent with the magnetic reflection becoming broader and weaker as the Dy concentration falls. For the $x = 0.2$ alloy (figure 5 inset) the temperature-dependent scattering without the temperature-independent ridge subtracted is displayed. The magnetic scattering in this case is rather broad. If the Dy and Pr moments are antiparallel for the reasons discussed in the introduction, the average moment is zero for $x = 0.24$. The moments will then be small for $x = 0.2$ and 0.3 but large for $x = 0.05$, 0.13 and 0.4.

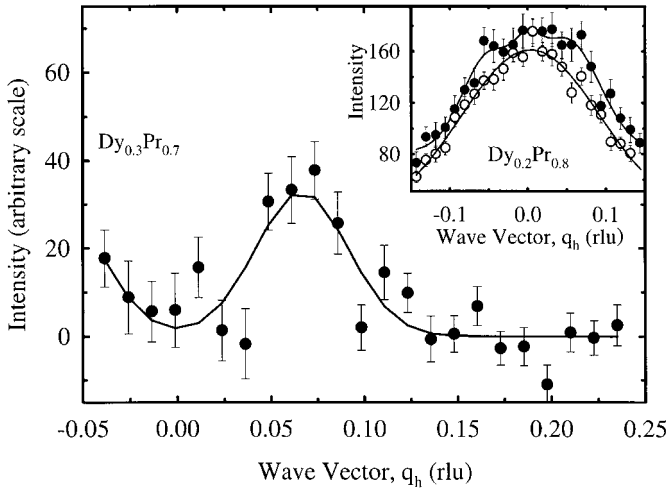

Figure 5. The magnetic scattering for $\boldsymbol{Q} \sim (q_h\ 0\ 3/2)$ from $Dy_{0.3}Pr_{0.7}$. Inset: the neutron scattering intensity measured in scans of $\boldsymbol{Q}$ along $[q_h\ 0\ 3/2]$ at 6 K (full circles) and 45 K (open circles) for $Dy_{0.2}Pr_{0.8}$.

Despite exhaustive searches, no magnetic diffraction peaks could be detected for the $Dy_{0.13}Pr_{0.87}$ or $Dy_{0.05}Pr_{0.95}$ alloys. A variety of scans of $\boldsymbol{Q}$ were attempted in the $(q_h\ 0\ q_l)$ plane, particularly sampling regions where magnetic peaks have been observed in other dhcp rare-earth elements. From this and references [9] and [20] it appears that moderate concentrations of Dy or Ho in Pr or Nd inhibit magnetic order.

To further investigate the suppression of magnetic order, magnetization measurements were made on the $Dy_{0.13}Pr_{0.87}$ alloy. The measurements were made between 2 K and 25 K in a 500 Oe field applied parallel to the basal plane and are shown in figure 6. The sample was first cooled in the absence of a magnetic field and the magnetization measured while warming (the zero-field-cooled curve in figure 6). Then the magnetization was measured while cooling in the 500 Oe field; this is shown as the field-cooled curve. The field was removed and the thermo-remanent magnetization was recorded as the sample warmed up. The results, figure 6, showed a clear spin-glass signature [21]. The spin-glass freezing temperature is $T_g = 12 \pm 1$ K.

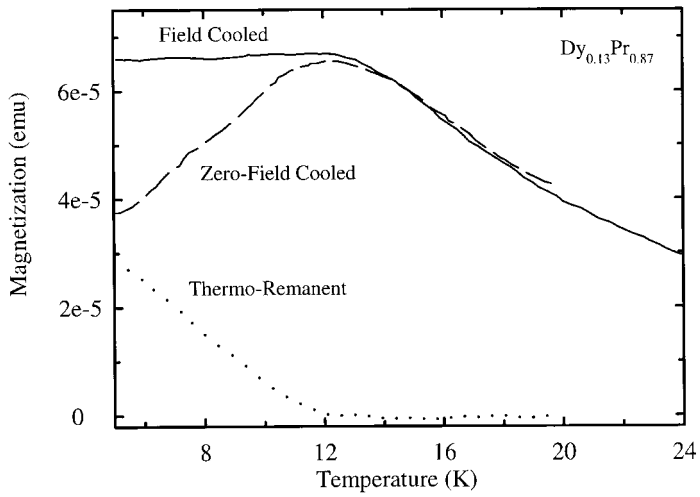

Figure 6. Magnetization results for the dhcp alloy $Dy_{0.13}Pr_{0.87}$. This, combined with field-sweep results, identifies the sample as a spin glass. The spin-glass freezing temperature is $T_g = 12 \pm 1$ K.

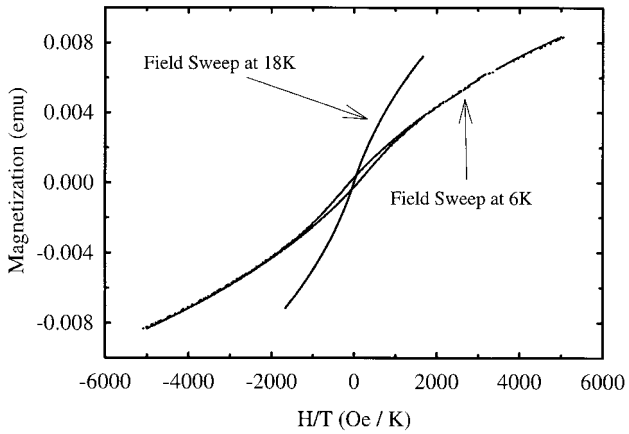

Figure 7. Field-sweep magnetization results at two temperatures for the dhcp alloy $Dy_{0.13}Pr_{0.87}$. Hundreds of spins operate together above the transition, far fewer than in a conventional superparamagnet.

Field-sweep magnetization results for $Dy_{0.13}Pr_{0.87}$ are presented in figure 7. The change in slope and the occurrence of hysteresis show the departure from Curie-law behaviour at low temperatures. The gradient of the curve above the spin-glass freezing temperature can be used to show that clusters containing less than ten sites are operating together [14]. These are smaller than expected for a conventional superparamagnet and smaller than the structural clusters. The combination of this and the lack of long-range ordering shown with neutron scattering suggests that the system is a spin glass.

The neutron scattering results for the more concentrated samples could also be symptomatic of spin-glass behaviour. Incommensurate short-range-order peaks similar to those observed for $Dy_{0.4}Pr_{0.6}$ have been measured by neutron scattering for the canonical spin-glass system CuMn [13]. It was found in this case that the spin-glass freezing temperature

as determined from the temperature dependence of the diffuse scattering was more than double that found using thermodynamic techniques. On improving the energy resolution of the measurements, the onset of magnetic scattering began to move towards the anticipated temperature. Here the energy resolution was $\Delta E \sim 0.2$ meV which is comparable to the lowest energy resolution employed in reference [13] and some proportion of inelastic scattering can be expected. The transition temperatures presented for this sample should not be compared with a spin-glass freezing temperature obtained from the much lower-frequency magnetization measurements.

3.2.2. Er_xPr_{1-x}. The magnetic scattering observed for $\boldsymbol{Q} \sim (q_h\ 0\ 3/2)$ from $Er_{0.05}Pr_{0.95}$ is shown in figure 8(a). The temperature dependence of the integrated intensity of this peak is shown in figure 8(b). The ordering temperature deduced from these results is 3.4 ± 0.5 K which is more than 50 times higher than that for bulk Pr. The ordering wave vector has also been considerably shifted to higher q_h compared to that for the pure element. The position of the magnetic peak remains fixed as the temperature is varied and no broad component was observed, although it has been for a bulk sample with nominally the same composition [6]. At 1.8 K the magnetic intensity is consistent with a modulated structure in the basal plane with the Er moments aligned in the *c*-direction. Similar magnetic scattering was also observed for a sample of composition $Er_{0.1}Pr_{0.9}$. In this case the ordering temperature and wave vector are nominally larger (table 1). At 1.8 K the magnetic correlation lengths in the basal plane for $Er_{0.05}Pr_{0.95}$ and $Er_{0.1}Pr_{0.9}$ were 220 ± 22 Å and 250 ± 25 Å respectively. The in-plane structural coherence length, measured from the (0 0 2) reflection, is 360 ± 5 Å and this indicates that the system is close to being in a long-range-ordered state.

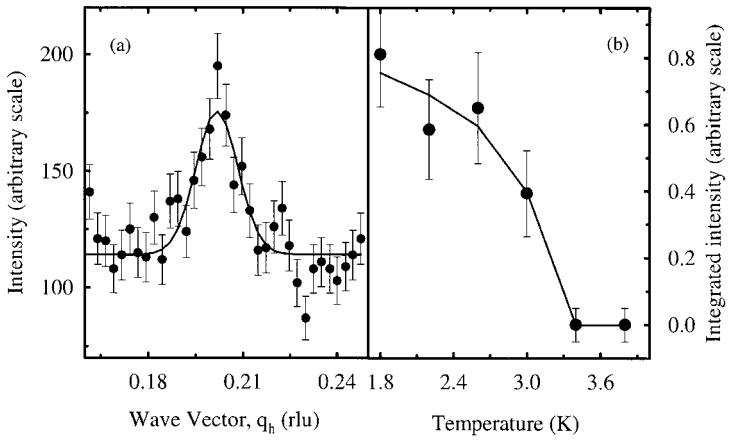

Figure 8. (a) The magnetic scattering observed for $\boldsymbol{Q} \sim (q_h\ 0\ 3/2)$ from $Er_{0.05}Pr_{0.95}$. (b) The temperature dependence of the peak intensity, showing that the ordering temperature is 3.4 ± 0.5 K.

For the two samples Er_xPr_{1-x} with $x = 0.05$ and 0.1 it is assumed that, as with Pr, the magnetic order occurs first on the hexagonal sublattice. This assumption is based on existing measurements: Rainford *et al* studied the magnetic behaviour of bulk single-crystal $Er_{0.05}Pr_{0.95}$ [6]. At around 5 K a broad diffuse peak was observed with $\boldsymbol{Q} \sim (0.15\ 0\ 3/2)$. Long-range order was observed below $T_N = 2.4$ K with $\boldsymbol{Q} \sim (0.20\ 0\ 3/2)$. The ordering wave vector is significantly larger than that in pure Pr, while the ordering temperature is also much higher. This alteration was associated with the doublet ground state of Er which was taken to lead to the polarization of the host electronic system. Additionally, the magnetic excitations

were measured at 4 K along ΓA and ΓM directions in reciprocal space. The lowest optical branch in the ΓM direction was observed and in the alloy the minimum excitation energy is significantly lower than in pure Pr and has its maximum at a larger wave vector (0.2 rlu). The fact that the lowest-energy excitation dispersion is simply a modified version of that observed in Pr suggests that the magnetism of this alloy is still dominated by the moments on the hexagonal sublattice. The acoustic modes were measured close to the (0 0 2) and the optical modes were measured close to the (0 0 3/2). This choice of wave vector suggests that the excitations are polarized in the basal plane. An impurity mode was measured which perturbed the host excitons where modes crossed. This mode was associated with a crystal-field excitation from the ground-state doublet of the Er impurity to an excited doublet.

Neutron scattering measurements were carried out on a further alloy of composition $Er_{0.2}Pr_{0.8}$. In this case no magnetic scattering was observed despite a thorough search throughout the $(q_h\ 0\ q_l)$ plane. It is possible that the magnetic order was not measurable because the moment from the Er and that from the Pr were close to complete cancellation.

4. Model results

The short-range order observed via neutron scattering measurements for some of the Dy_xPr_{1-x} alloys and the magnetization measurements for $Dy_{0.13}Pr_{0.87}$ suggest that these systems are spin glasses. In the ground state of a spin glass the moments are frozen in a random configuration. The necessary conditions are that there must be both competition between different interactions and randomness. Since the systems discussed here are alloys, randomness exists. To explain the observed suppression of long-range order in the Dy alloys, the nature of the two-ion coupling in light–heavy alloys has to be considered. In particular, the role of the dipole–dipole interaction is evaluated here.

The observed behaviour can be discussed in terms of the Mattis model [22]. The Mattis model contains randomness but no frustration [23]. As a consequence it has an ordinary continuous phase transition. The Hamiltonian is

$$\mathcal{H} = -\sum_{ij} \mathcal{J}(R_{ij})\varepsilon_i\varepsilon_j \boldsymbol{S}_i \cdot \boldsymbol{S}_j - h\sum_i S_{iz}. \tag{5}$$

The coupling is given by $\mathcal{J}(R_{ij})\varepsilon_i\varepsilon_j$ where ε_i and ε_j are random variables with $\varepsilon_i = \pm 1$. New variables can be defined:

$$\boldsymbol{\tau}_i = \varepsilon_i \boldsymbol{S}_i \tag{6}$$

with which the Hamiltonian becomes

$$\mathcal{H} = -\sum_{ij} \mathcal{J}(R_{ij})\boldsymbol{\tau}_i \cdot \boldsymbol{\tau}_j - h\sum_i \varepsilon_i \tau_{iz}. \tag{7}$$

Now the Hamiltonian is composed of a pseudospin-coupling term and a random Zeeman term. If there is no applied field then all randomness disappears. Rather than showing spin-glass behaviour, the system has a ground state with the τ-variables fully aligned. The original S-spins are randomly oriented but this does not affect the critical behaviour of the system. This simple model illustrates that competing $\mathcal{J}(R_{ij})$ are necessary for a system to be a spin glass. In a conventional spin glass there is a low concentration of spins and the host is a noble metal. The sign of the RKKY coupling changes with distances R_{ij} between spins. These distances are random and so the sign of the coupling changes randomly, leading to competing interactions. In the light–heavy-rare-earth alloys there are spins on every site. An exchange interaction without random distances is analogous to the $\mathcal{J}(R_{ij})\varepsilon_i\varepsilon_j$ interaction described above. The random variables ε_i can be thought of as taking the values +1 for a heavy-rare-earth spin and

-1 for a light rare earth. Rewriting the problem in terms of pseudospins, it is clear that such a system would not be frustrated.

The dipole–dipole interaction is important in light–heavy-rare-earth alloys because, unlike the indirect exchange interaction, it couples the total moments. In heavy rare-earth metals and their alloys the dipole–dipole interaction is very small compared to the indirect exchange. In light rare-earth metals and the alloys discussed here the ordering temperatures tend to be of the order of a few kelvins and the dipole–dipole interaction becomes more significant. As was discussed in the introduction, the two constituents have $\boldsymbol{J} = |\boldsymbol{L} - \boldsymbol{S}|$ and $\boldsymbol{J} = \boldsymbol{L} + \boldsymbol{S}$ moments respectively which causes the dipole–dipole interaction to compete with the exchange interaction which couples the spins. In the dhcp light rare earths the moments are reduced and the influence of the indirect exchange decreases, leading to increased importance for the dipole–dipole interaction. The energy contribution is

$$E = \frac{1}{2}\sum_{ij} \frac{\boldsymbol{\mu}_i \cdot \boldsymbol{\mu}_j}{|r_{ij}|^3} - \frac{3(\boldsymbol{\mu}_i \cdot \boldsymbol{r}_{ij})(\boldsymbol{\mu}_j \cdot \boldsymbol{r}_{ij})}{|r_{ij}|^5}. \tag{8}$$

In the case of the rare earths the ordered magnetic structures tend to have moments with incommensurate modulations:

$$\boldsymbol{\mu}_i = \boldsymbol{\mu} \mathrm{e}^{-\mathrm{i}\boldsymbol{k}\cdot\boldsymbol{r}_i}. \tag{9}$$

Evaluating the contribution due to the dipole–dipole interaction by truncating it to a few nearest neighbours leads to problems. It is a slowly diminishing highly anisotropic interaction. Before evaluating this expression, a qualitative indication of its effect will be outlined.

Qualitatively the dipole–dipole interaction is known to make longitudinal fluctuations more energetic due to the macroscopic field that they create. The longitudinally modulated magnetic structures for the light rare-earth metals Pr and Nd would appear to be raised in energy by this macroscopic field. The magnetic structures of Pr and Nd involve a longitudinal modulation for which the moment and the incommensurate modulation wave vector lie in the basal plane; however, successive hexagonal planes are stacked antiferromagnetically. Due to this antiferromagnetic alignment, the magnetic unit cell contains magnetic moments in two planes which are aligned antiparallel. The macroscopic field from the pairs of moments cancels, reducing the dipolar contribution to the energy for this ordered structure. The magnetic structures of Pr and Nd appear to be responding to the dipole–dipole interaction. The antiferromagnetic alignment of the hexagonal planes in the dhcp alloys results in the magnetic scattering being located around $q_l = 1/2$ or 3/2.

The dipole–dipole interaction decreases with distance as $1/r^3$ and is highly anisotropic. Accurate evaluation requires a calculation for an infinite lattice. In practice this is achieved by dividing the summation over all dipoles into a sum over neighbouring dipoles carried out in configuration space and a second sum over distant dipoles carried out in reciprocal space [24]. The radius at which the configuration-space/reciprocal-space division is made is a matter of trial and error with a good choice leading to two summations which separately converge quickly. The expressions are given in references [25] and [26].

The summations have been carried out for a magnetically ordered dhcp-crystal-structure material. The magnetic behaviour of these systems tends to be dominated by the hcp hexagonal sublattice. In keeping with this, only the moments on the hexagonal sites have been considered. The results for modulation vectors along $[q_h\ 0\ 3/2]$ are presented in figure 9. The lattice parameters and energy scale are those appropriate to dhcp Pr and the magnetic structures have planes which are antiferromagnetically aligned in the same way as Pr, Nd and the alloys studied here. In order to facilitate comparison with the alloys, the right-hand axis gives the energy scale that would be used if this was the same lattice but with Dy magnetic moments. Figure 9 shows that the dipole–dipole interaction in a $\mathrm{Dy}_x\mathrm{Pr}_{1-x}$ alloy will have a major influence below 5 K.

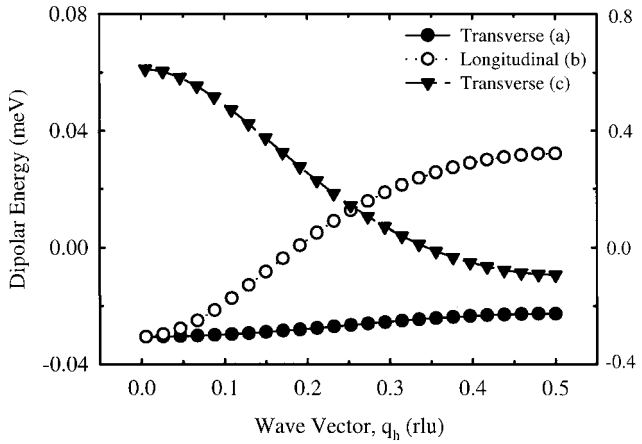

Figure 9. The calculated dipolar contribution to the interaction energy for magnetic ordering on the hexagonal sites, where successive hexagonal planes are aligned antiferromagnetically. The energies are plotted as a function of wave vector, q_h, for moments aligned along the a-direction (filled circles), b-direction (empty circles) and c-direction (triangles). The scale on the left (right) axis gives the energy for Pr (Dy).

The highest-energy modes in figure 9 are the transverse (c) mode at small q_h and the longitudinal (b) mode at large q_h. This is in keeping with the macroscopic field cancelling for successive antiferromagnetically aligned planes. That magnetic scattering occurs at (q_h 0 3/2) and (q_h 0 1/2) is likely to be due to the influence of the dipole–dipole interaction on the dhcp light rare-earth metals Pr and Nd.

5. Discussion

The x-ray diffraction studies of the dhcp alloys reveal sharp superlattice peaks along the [0 0 q_l] and the neutron diffraction also shows diffuse scattering along the same axis. The former are due to variations in the distribution of the constituents within the four planes of the unit cell, while the latter appears to be due to small strain domains which lead to uncorrelated changes in the plane spacing. The x-ray form-factor variation is of the order of 2%, which sounds insignificant; however, this implies concentration variations between cubic and hexagonal symmetry planes of tens per cent which is non-negligible. It seems highly likely that the heavy-rare-earth ions will tend to prefer the hexagonal symmetry sites due to the similarity to the hcp crystalline environment.

The dhcp light–heavy-rare-earth alloys exhibit a range of magnetic behaviour due to competition between different two-ion interactions and the crystal-field anisotropy. For the Dy_xPr_{1-x} alloys magnetic neutron scattering corresponding to short-range order has been observed for concentrations above $x = 0.2$. The correlation length for the magnetic order increases with concentration x. At $x = 0.13$ magnetization measurements suggest spin-glass behaviour. The uniaxial alloy system Er_xPr_{1-x} was also studied. Neutron scattering measurements reveal order with a correlation length close to that for the chemical structure for $x = 0.05, 0.1$ while at $x = 0.2$ there was approximate cancellation of moments. Alloys of compositions with x as high as 0.4 were not studied.

Frustration is a necessary condition for spin-glass behaviour. For the light–heavy-rare-earth alloys competing interactions are a consequence of the spin–orbit interaction. The light

rare earths have $\boldsymbol{J} = |\boldsymbol{L} - \boldsymbol{S}|$ coupling while Dy, Ho and Er have $\boldsymbol{J} = \boldsymbol{L} + \boldsymbol{S}$. When the spins order magnetically via the indirect exchange, the bulk of the moments of the two constituents are aligned antiparallel. It has been shown here that under these circumstances the dipole–dipole interaction will compete by favouring alignment of the total moment. Lattice sum calculations have been performed. These show that the dipolar energy will be significant below 5 K. The wave-vector dependence of the dipole–dipole interaction concurs with the neutron scattering results presented here. Magnetic scattering was found for the easy-plane $Dy_{0.3}Pr_{0.7}$ and $Dy_{0.4}Pr_{0.6}$ alloys around (0.06 0 3/2). The longer-range-order peaks for uniaxial $Er_{0.05}Pr_{0.95}$ and $Er_{0.1}Pr_{0.9}$ alloys had an ordering wave vector (0.20 0 3/2). These modulation wave vectors are evenly spread either side of the modulation wave vector for dhcp Pr which is (0.128 0 3/2). The augmented dipole–dipole contribution which is introduced with the heavy-rare-earth moment is responsible for the change in wave vector. As can be seen in figure 9, the easy-plane modes favour low modulation wave vector while the uniaxial mode has lower energy at a higher ordering wave vector. The anisotropy due to the crystal field and the dipole–dipole competition combine to give the observed order.

There is a clear difference between the behaviours of the Er_xPr_{1-x} alloys compared to those of Dy_xPr_{1-x}. The former give close to long-range order for small x while the latter still only exhibit short-range order for $x = 0.4$. This difference in magnetism for these two systems may stem from the numbers of components in each order parameter. The hexagonal crystal field makes Er uniaxial while Dy is an easy-plane system. The number of possible ordered magnetic structures is higher for the latter, leading to an increased chance of frustration.

A similar relationship between long-range order and the number of components in the order parameter occurs in random-field systems [27]. Here the system either forms a long-range-ordered structure or it breaks up into domains making the order parameter zero. Ising and XY systems behave differently because the energy cost of forming a domain wall changes. In an Ising system, up and down spins will be nearest neighbours, whereas in an XY system, the wall can have width and the moments rotate over a number of sites. Domain formation is much more likely for the XY system. An Ising system in a random field will break up into domains if the dimension of the system $d < 2$ and for the XY system for $d < 4$. It is also more viable for the XY system to break up into small ordered regions for light–heavy-rare-earth alloys than it is for Ising alloys.

Acknowledgments

This research was aided by the technical expertise of the staff at Risø National Laboratory. Financial support was provided by the EPSRC in the UK and by the EU under its Large Installations Programme in Denmark.

References

[1] Clegg P S, Cowley R A, Goff J P, McMorrow D F, Ward R C C and Wells M R 2001 *J. Phys.: Condens. Matter* **13** 10175–89
[2] McEwen K A and Stirling W G 1981 *J. Phys. C: Solid State Phys.* **14** 157–65
[3] Bjerrum Møller H, Jensen J Z, Wulff M, Mackintosh A R, Masters O D and Gschneidner K 1982 *Phys. Rev. Lett.* **49** 482–5
[4] Touborg P 1977 *Phys. Rev.* B **16** 1201–11
[5] Coles B R 1984 *J. Less-Common Met.* **100** 93–103
[6] Rainford B D, Cussen L, Jensen J and Fort D 1988 *J. Magn. Magn. Mater.* **76+77** 399–400
[7] Steigenberger U, McEwen K A and Jensen J 1995 *Physica* B **213+214** 324–6
[8] Sarthour R 1999 *DPhil Thesis* University of Oxford

[9] Goff J P, Bryn-Jacobsen C, McMorrow D F, McIntyre G J, Simpson J A, Ward R C C and Wells M R 1998 *Phys. Rev.* B **57** 5933–40
[10] Everitt B A, Salamon M B, Borchers J A, Erwin R W, Rhyne J J, Park B J, O'Donovan K V, McMorrow D F and Flynn C P 1997 *Phys. Rev.* B **56** 5452–60
[11] Mydosh J A 1993 *Spin Glasses: an Experimental Introduction* (London: Taylor and Francis)
[12] Violet C E and Borg R J 1966 *Phys. Rev.* **149** 540–51
[13] Werner S A, Rhyne J J and Gotaas J A 1985 *Solid State Commun.* **56** 457–60
[14] Bean C P and Livingstone J D 1959 *J. Appl. Phys.* **30** 120S–4S
[15] Cowley R A, Ward R C C, Wells M R, Matsuda M and Sternlieb B 1994 *J. Phys.: Condens. Matter* **6** 2985–98
[16] Jain S C, Harker A M and Cowley R A 1997 *Phil. Mag.* A **75** 1461–515
[17] Guinier A 1959 *Solid State Physics* vol 9 (New York: Academic) pp 294–398
[18] Cohen J B 1986 *Solid State Physics* vol 39 (New York: Academic) pp 131–206
[19] Koch C C 1970 *J. Less-Common Met.* **22** 149–73
[20] Chatterjee D and Taylor K N R 1972 *J. Phys. F: Met. Phys.* **2** 151–8
[21] Nagata S, Keeson P H and Harrison H R 1979 *Phys. Rev.* B **19** 1633–8
[22] Plischke M and Bergersion R 1994 *Equilibrium Statistical Physics* (Singapore: World Scientific)
[23] Mattis D C 1976 *Phys. Lett.* A **56** 421–2
[24] Born M and Huang K 1954 *Dynamical Theory of Crystal Lattices* (Oxford: Oxford University Press)
[25] Aung S and Strauss H L 1973 *J. Chem. Phys.* **58** 2737–45
[26] Cohen M H and Keffer K 1955 *Phys. Rev.* **99** 1128–34
[27] Imry Y and Ma S K 1975 *Phys. Rev. Lett.* **35** 1399–401